Key Aspects of Robot based Antenna Measurements at Millimeter Wave Frequencies

Martin Hitzler[1], Sebastian Bader[1], Christian Waldschmidt[1],
[1]Institute of Microwave Techniques, University of Ulm, Ulm, Germany, firstname.lastname@uni-ulm.de

***Abstract*—In this paper important aspects concerning a probe based antenna characterization environment for frequencies up to 325 GHz are described. The flexibility to measure the far-field antenna diagram and to perform a near-field sampling is achieved by use of an industrial robot. In advance to the complete measurement setup verification, two main aspects of the new system are investigated. For the measurement of an antenna radiation pattern the receiving frequency converter is moved around the probe station with the Antenna Under Test (AUT). Therefore, the cables carrying the intermediate frequency signal are also in motion. The impact on the accuracy of the results is shown. Moreover an antenna gain calibration technique with a 3S-standard (three Shorts) for the probe deembedding and its precision are discussed.**

***Index Terms*—millimeter wave frequencies, integrated antenna measurements, robot based antenna measurements, probe based antenna measurements, calibration stability.**

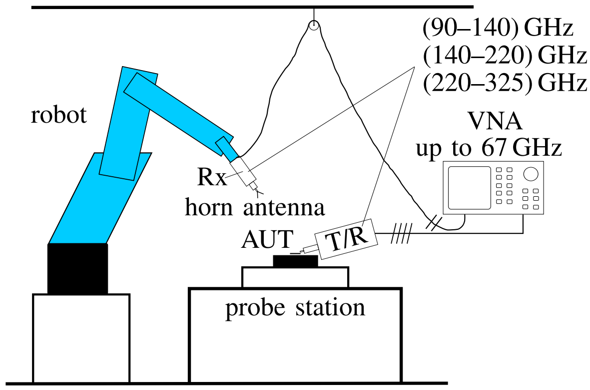

Fig. 1. Schematic measurement setup with a receiver module mounted at the robot.

I. Introduction

Wafer based measurements with probe tips at millimeter wave frequencies are state-of-the-art. The increasing operating frequency of many RF-systems creates a demand for the characterization of their radiating elements on chip. Therefore, several mechanical assembly solutions for measuring the gain and radiation pattern of antennas in the millimeter wave range were built and evaluated [1]–[6]. A fundamentally different concept was proposed recently from the NIST [7]. The authors use a robot to move the receiving antenna and reported the geometrical accuracy of their robotically controlled antenna measurement system. We extended this setup towards the measurability of integrated antennas on a probe station.

In a robot supported antenna measurement environment, as shown in Fig. 1, the antenna far-field and near-field are characterized by moving the receiving antenna in almost all reasonable 3D-shapes like hemispheres and planes. The far-field condition depends on frequency and antenna aperture. The robot offers the degree of freedom to adjust the distance between the antennas as desired and needed. According to that at very high frequencies the best dynamic range can be achieved easily. The AUT on the probe station is connected to a Transmit/ Receive (T/R) converter via a waveguide-fed probe. The receiving horn antenna is joined with a receiving converter module (Rx) being considerably smaller than a T/R converter module. This receiving assembly is mounted at the robot hand. Both converters are connected with cables to a Vectorial Network Analyser (VNA). These cables have to be moved during a radiation pattern measurement causing unquantified degradation of the calibration and the results. Therefore, an investigation was carried out to get a quantitative measure of the scattering parameters when cables are moving.

In the first part of this paper, the cable influences are analyzed with an approach of the converter's functional principle and measured for different cable types and scenarios. In the second part, a gain calibration technique suitable for a robot based antenna measurement with a probe station is performed.

II. Calibration Stability at Cable Movements

In this work, the converter modules in the E-Band (60 GHz to 90 GHz) are used for cable investigations because these provide the highest frequency range available in our institute. Measurements at higher frequencies using the robot will be evaluated as soon as the appropriate equipment is installed.

The critical scattering parameters for cable movements can be identified from the functional principle of the converter modules and the VNA shown in Fig. 2. Two signals, named RF and LO, are required to feed the converter. The reference (REF) and measured (MEAS) signals are at 300 MHz and for this reason comparatively uncritical for cable movement. A change of an RF cable does not have an influence on the measurement result because the scattering parameters are determined as MEAS-to-REF ratios so that the errors are compensated. For the LO cable this is only true for the reflection coefficient. In the transmission path the REF signal is generated with a different LO signal than the MEAS signal.

978-88-907018-4-9/14/$31.00 ©2014 IEEE

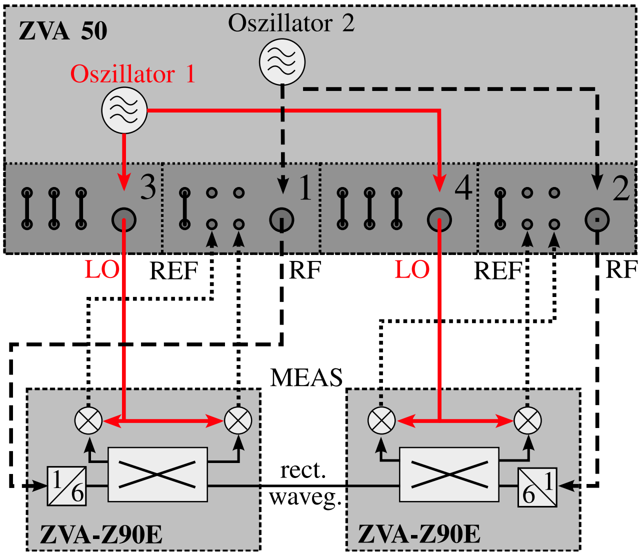

Fig. 2. Functional principle of two E-Band converter modules connected to a VNA [8].

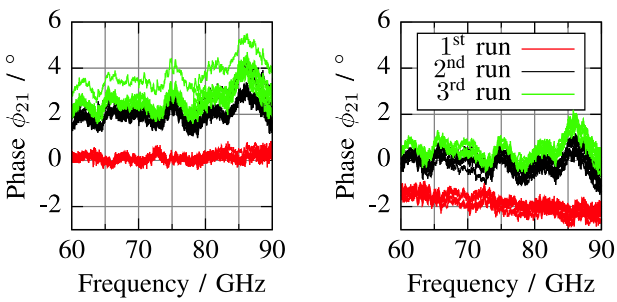

(a) Lower level.

(b) Upper level.

Fig. 3. Phase shift of the transmission coefficient s_{21} for an alternating cable lifting and lowering.

Therefore, a movement of the LO cable will modify the results of the transmission coefficients. For that reason, only the transmission coefficient is considered in the following measurement scenarios.

A. Lifting and Lowering of Cables

Simple movements like cable shifting affect mainly the bend radius of the cable causing a phase change. Consequently, only the phase shift of the transmission coefficient ϕ_{21} is investigated. In the amplitude no significant change was measured. In a first test a 91 cm long ZV-Z193 cable [8] was alternately lifted and lowered with a hub of 10 cm. Three runs of 15 measurements were carried out depicted in Fig. 3. The repeatability within one series is better then 1°. The induced phase difference between the lower and the upper level is approximately 2°–3°. In Fig. 3(b) only the first measurement in the third series has a higher absolute phase level. This shows the so-called memory of the cable. After the first lifting and lowering the cable takes in each state nearly the same position and shape giving the mentioned repeatability.

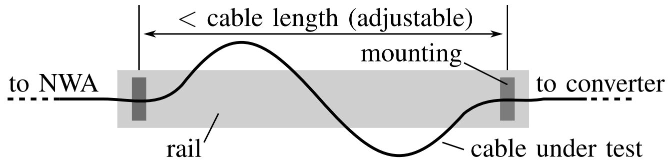

Fig. 4. Mounting of the cable on a rail.

B. Comparison of Different Cable Types

In a second measurement procedure three longer cables are compared to each other. The moveable cable length could be adjusted from 70 cm to 110 cm on a rail as presented in Fig. 4. The distance between the fixing points is tunable so that e.g. for longer moveable cable parts the distance is larger. As in the first scenario 15 individual measurements are carried out for each cable and for each length. The mean value of the phase differences between the lower and the upper level is demonstrated in Fig. 5. The 3 m Sucoflex_103 from Huber & Suhner [9] is the cable with the largest stiffness and thus the largest memory with respect to movements. The 110 cm long part has the tightest S-shape since the distance of the fixing points was smaller than in the other measurements. Consequently, the slope is the largest one of the nine regression lines. The gradient is lower for the 70 cm and the 90 cm long cable because of the larger bend radii. The 6 m True Blue 125 (type: 421-011) cable from Teledyne Storm [10] has a comparable rigidity and increasing bend radii for increasing length of the moveable cable part resulting in slightly lower slopes. The smallest gradient appears for the 8 m RTK 106 cable from Rosenberger [11], which is the most flexible cable being tested. From this investigation, the most flexible cable has the lowest phase shift in this scenario.

C. Reproduction of a Hemispherical Cable Movements

In the next setup shown in Fig. 6 the cable movement for a radiation pattern measurement is imitated. For this purpose one LO signal path was guided over the coupling path of a directional coppler to the cable under test. Over a pulley on the ceiling the test cable is led to a short circuit mounted on a moveable bar. It can be rotated in the horizontal plane with ϕ_{pol}=0° or 90° and in the vertical plane with θ=−90° . . . 90°. The reflected signal over the main path of the coupler can be adjusted in the power level with an amplifier and an attenuator. Due to the reflection the phase difference is measured with the doubled value and is already corrected.

The results presented in Fig. 7 are for clarity purpose only regression lines of the phase difference between the top position at θ=0° and other positions. For the black dashed line the plot results are strongly different in dependence to ϕ_{pol}. This is caused by the predominent direction of the pulley and the cable. Without this effect all four black curves should have approximately the same amount of phase difference which should be the biggest offset for all angles θ. From a geometrical point of view this means e.g. that for θ=90°

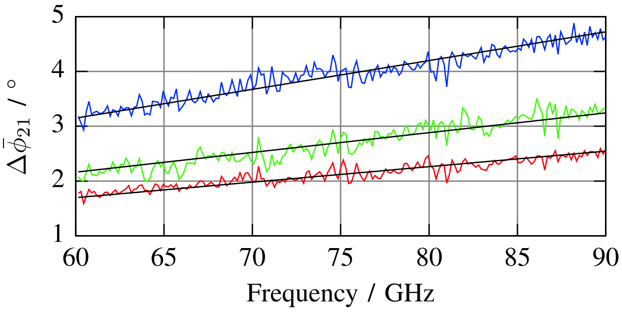

(a) 3 m Sucoflex_103 from Huber & Suhner [9].

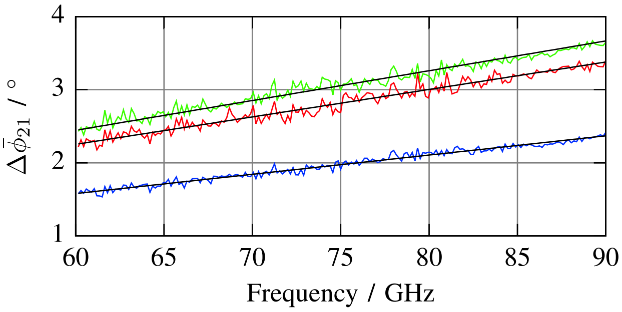

(b) 6 m True Blue 125 (type: 421-011) from Teledyne Storm [10].

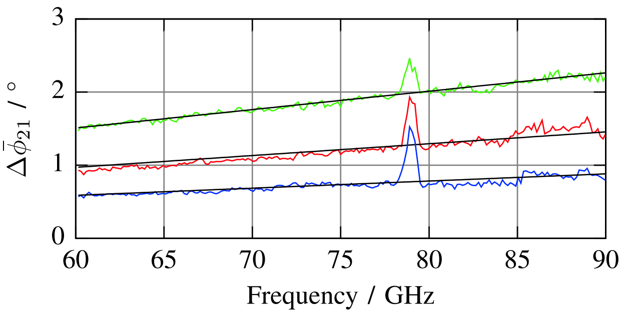

(c) 8 m cable (type: RTK 106, connector: RPC-2.92) from Rosenberger [11].

Fig. 5. Mean value of the phase shift of the transmission coefficient for three different cables and the lengths 70 cm —, 90 cm —, 110 cm — with the corresponding regression lines.

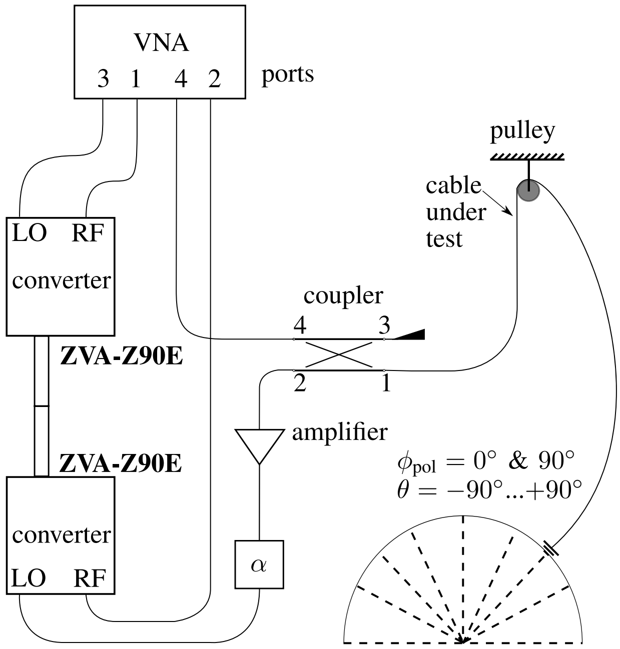

Fig. 6. Setup for the reproduction of the influence of the cable movements on a radiation pattern measurement.

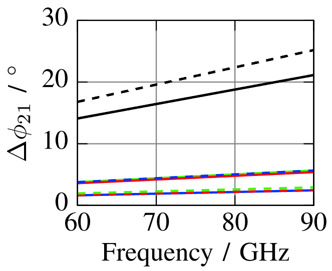

(a) $\phi_{pol} = 0°$.

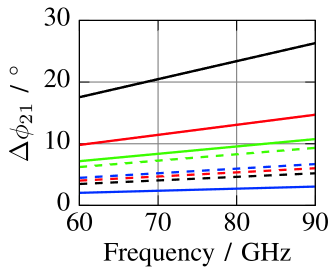

(b) $\phi_{pol} = 90°$.

Fig. 7. Regression lines of the phase difference ϕ_{21} between θ=0° and 90° —, −90° - - -, 60° —, −60° - - -, 45° —, −45° - - -, 30° —, −30° - - -.

the cable is in an S-shape and for θ=−90° it is in a wide circular shape. Consequently, for a robot based radiation pattern measurement the cable and its mounting should have a minimum predominant direction and shape. Furthermore, the huge increase of phase shift for θ=±90° is additionally enforced by the tension of the cable.

D. Scalability for Millimeter Wave Frequencies

The phase shifts can be scaled in frequency since the signal is multiplied with the corresponding factor to convert it into the desired band. The regression curves are lines through the origin and are therefore fully characterized by their slope. The expected phase shift for the 8 m Rosenberger cable in Fig. 5(c) at 325 GHz would be about 3°– 4°, which is a negligible small value. For the imitation of the cable movement at the antenna measurement environment with the robot a phase shift of about 90° at 325 GHz would occur if the cable stress and tension is not reduced. For a minor phase offset of 15° as shown with the red line in Fig.7(b) the scaling predicts 54°. Consequently, a flexible cable with a sophisticated guidance and mounting results in smaller phase errors.

From a theoretical point of view the phase error for gain measurements is less severe than an amplitude error. The variance of the absolute value in the measurements was less than 0.1 dB, and an increase with respect to frequency is not expected. That means amplitude measurements with cable movements appear realizable with acceptable accuracy. In contrast to that for near-field scans the cable movement is significantly smaller like in the first scenario resulting in expected phase offsets under 10° at 325 GHz. In the following chapter a suitable calibration method for the determination of the antenna gain is evaluated.

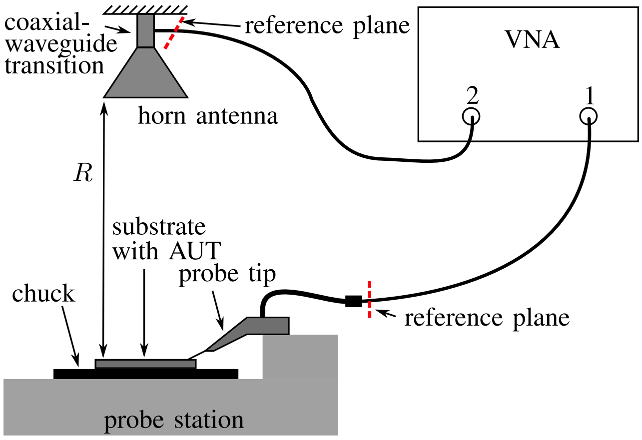

Fig. 8. Setup for gain measurements with a probe station.

III. Gain Calibration Methods Suitable for Robot Based Antenna Characterization

In this chapter the three required steps for the determination of the antenna gain [12] and possible accuracy enhancements are discussed. An overview of the measurement setup gives Fig. 8. The reference planes of the VNA are at the end of the cables for the following calibration example. For a setup with converter modules the reference plane would be at the end of the rectangular waveguide. In the first part two identical Ka-Band horn antennas, each with coaxial to waveguide transition, are measured to determine the gain of a horn with an adapter. The deembedding of the probe is described in the following section.

A. 3S-Calibration Method

The most popular one-port calibration method is the Short Open Load (SOL) calibration. The determination of the parasitic elements of the standards for planar circuits at frequencies up to 325 GHz integrated in most cases on a chip can be difficult. The 3S-calibration method is probably more suitable for this one-port calibration since only one kind of termination is required. The three standards are built by one ordinary short-circuit and two short-circuited offset transmission lines shifting the phase of the three reflections [13]. To evaluate the deembedding a simple microstrip-fed patch antenna on a Rogers *RO*3003 substrate was fabricated resonating at 40 GHz. After the measurement of the three standards and the antenna, the reflection coefficient can be calculated. Figure 9 shows the measured reflection coefficient in comparison to the simulation. The curves prove that the calibration works and the probe can be deembedded. Knowing the error terms of the probe, its gain G_{probe} can be determined as the product of the transmission error terms e_{01} and e_{10} [12]. In the third step the calculation of the gain is possible.

B. Gain calculation

The transmission chain with its scattering parameters and the corresponding factors is demonstrated in Fig. 10. The gain of the AUT G_{AUT} can be determined with the distance R, the gain of the probe G_{probe}, the smoothed gain of the receiving horn antenna with the adapter G_{Rx} and the measured scattering parameter $s_{21,\text{tot}}$

$$G_{\text{AUT}} = \frac{|s_{21,\text{tot}}|^2}{G_{\text{probe}} G_{\text{Rx}}} \left(\frac{4\pi R}{\lambda_0}\right)^2. \tag{1}$$

A comparison between measurements with and without absorbing material on the chuck is presented in Fig. 11(a). Without absorbing material the gain curve suffers from an amplitude ripple of up to 4 dB resulting from the unshielded chuck. Using absorbing material around the antenna with a distance of about 2 mm the ripple can be reduced to less than 0.5 dB. To verify the approximated invariance of the amplitude with respect to cable movements, one cable is removed. According to this the short cable scenario consists only of two Agilent 85133F VNA cables [14] connecting the horn antenna and the adapter for the probe with the VNA respectively. In the long cable setup, an additional 1 m long Jyebao K30K30-5002-1M40 cable [15] is inserted between the horn antenna and the VNA. For both scenarios the cables are deembedded. The comparison is shown in Fig. 11(b). The difference between the curves shows the accuracy of the measurements with about 0.5 dB. In a last step the signal flow graph can be improved by including a loop between the antenna reflection coefficient s_{11} and the reflection of the probe, namely e_{11}, as highlighted in blue in Fig. 10. The result is depicted in Fig. 11(c) demonstrating changes in the vicinity of the resonance frequency. The differences show the destructive superposition of the loop signal with the direct signal causing a degradation of the gain if the loop is not considered. The maximum gain level is about 1 dB under the simulated value with CST Microwave Studio [16]. A reason for that can be the taper from the probe tip to the 50 Ω-transmission line on the PCB. The surface waves excited at

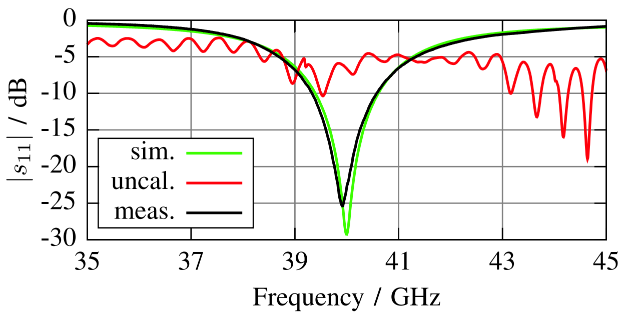

Fig. 9. Reflection coefficient of the test patch antenna.

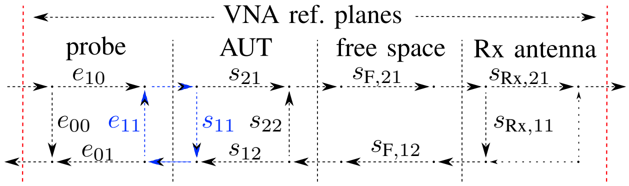

Fig. 10. Signal flow graph for gain determination.

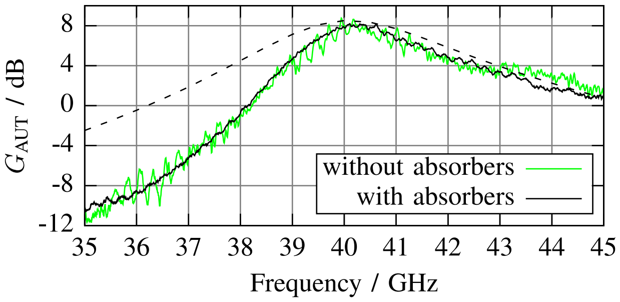

(a) Effect of absorbing material.

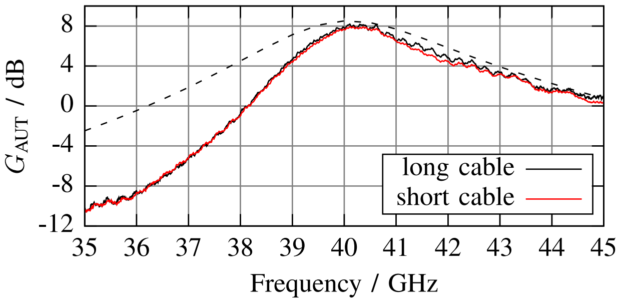

(b) Effect of cable length.

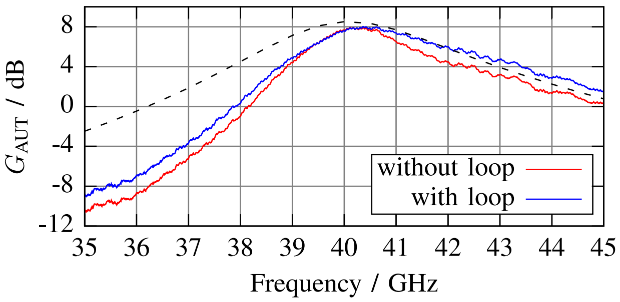

(c) Effect of signal flow graph refinement.

Fig. 11. Measured antenna gain (solid line) in comparison to the simulation (dashed line) for different effects.

this transition could not be taken into account in the simulation and can cause a little tilt of the main beam. This reduces the gain at broadside. Besides the need for absorbing material on the chuck, main results of the measurement procedure are, that the $3S$-calibration is very well suited to deembed the probe tip transition. By the use of the error parameters of the probe, the gain of the AUT can be determined, and additionally, the signal flow graph can be refined. This guarantees more accurate results in poorly matched regions of the AUT. With respect to the cables, a longer deembedded cable should cause only a quite small error in comparison to the overall measurement accuracy.

IV. Conclusion

The influence of cable movements on measurement results was shown for three different scenarios. Cable lifting and lowering causes a phase shift of about 1°–5° in the E-Band (60 GHz–90 GHz) depending on cable stiffness and moveable length. Because of the harmonic mixers in the frequency converters, the phase error will increase linearly with respect to frequency. Consequently, the expected phase error will be about 3°–20° at 325 GHz. With the correct choice of the cable, phase offsets under 5° are realizable at 325 GHz being acceptable for near-field scans with a scan area of e.g. 5 cm $\times$5 cm. For a circular cable movement in the presented setup, the expected phase shift is in the range of 25° at 90 GHz and extended to about 90° at 325 GHz. To decrease this variation, a cable mounting with no predominant direction is unavoidable. The amplitude variation caused by cable movements at 325 GHz is expected to be in the same region as for the E-Band with about 0.1 dB. Consequently for far-field scans, this error is usually tolerable.

The second part demonstrates an alternative one-port calibration method suited for probe deembedding. At gain measurements of a test antenna, the ripple could be reduced from 2 dB to less than 0.5 dB. The absolute difference between the simulated and measured gain is about 1 dB at the resonance frequency for broadside radiation. Its reasons are measurement tolerances and the assumed material losses.

References

[1] T. Zwick et al., "Probe based mmw antenna measurement setup," in *Antennas and Propagation Society International Symposium, 2004. IEEE*, vol. 1, 2004, pp. 747–750.
[2] T. Ito et al., "Radiation pattern measurement system for millimeter-wave antenna fed by contact probe," in *Microwave Conference, EuMC 2009. European*, 2009, pp. 1543–1546.
[3] S. Smith et al., "A millimeter-wave antenna amplitude and phase measurement system," *Antennas and Propagation, IEEE Transactions on*, vol. 60, no. 4, pp. 1744–1757, 2012.
[4] D. Titz, F. Ferrero, and C. Luxey, "Development of a millimeter-wave measurement setup and dedicated techniques to characterize the matching and radiation performance of probe-fed antennas [measurements corner]," *Antennas and Propagation Magazine, IEEE*, vol. 54, no. 4, pp. 188–203, 2012.
[5] A. Smolders et al., "Measurement and calibration challenges of microwave and millimeter-wave phased-arrays," in *Antenna Technology (iWAT), 2013 International Workshop on*, 2013, pp. 358–361.
[6] H. Gulan et al., "Probe based antenna measurements up to 325 GHz for upcoming millimeter-wave applications," in *Antenna Technology (iWAT), 2013 International Workshop on*, 2013, pp. 228–231.
[7] D. Novotny et al., "Performance evaluation of a robotically controlled millimeter-wave near-field pattern range at the nist," in *7th European Conference on Antennas and Propagation (EuCAP)*, 2013, pp. 4086–4089.
[8] ROHDE & SCHWARZ GmbH & Co. KG, Munich, Germany.
[9] HUBER+SUHNER AG, Pfaeffikon, Switzerland.
[10] Teledyne Storm Microwave, Woodridge, IL, USA.
[11] Rosenberger Hochfrequenztechnik GmbH & Co. KG, Fridolfing, Germany.
[12] S. Beer and T. Zwick, "Probe based radiation pattern measurements for highly integrated millimeter-wave antennas," in *4th European Conference on Antennas and Propagation (EuCAP)*, 2010, pp. 1–5.
[13] M. Thumm, *Hochfrequenzmeßtechnik Verfahren und Meßsysteme*. Teubner, 1997.
[14] Agilent Technologies, Inc., Santa Clara, CA, USA.
[15] JYEBAO HEADQUARTERS, Inc., Shin Juang City, Taipei Shien, Taiwan.
[16] CST Microwave Studio, Ver. 2012, CST AG, Darmstadt, Germany.